Int. J. Heat Mass Transfer. Vol. 5, pp. 915–928. Pergamon Press 1962. Printed in Great Britain.

MEASUREMENT OF LOW SPEED GAS FLOWS BY PARTICLE TRAJECTORIES: A NEW DETERMINATION OF FREE CONVECTION VELOCITY PROFILES*

R. EICHHORN†
Mechanical Engineering Department, Princeton University, Princeton, N.J. (U.S.A.)

(*Received* 29 *March* 1962)

Abstract—The development of a method for the measurement of small flow velocities and the application of this method to the measurement of free convection velocity profiles in air is described. The method employed uses photographic techniques to measure the trajectories of small dust particles ($d < 6{\cdot}6\,\mu$) carried along with the flow. Factors affecting the measurement technique and the results of the measurement of two laminar free convection velocity profiles on a vertical flat plate are presented.

NOMENCLATURE

Gr, Grashof No.;
g, acceleration of gravity;
β, coefficient of thermal expansion;
δ, boundary layer thickness;
ζ, dimensionless free convection stream tion;
η, dimensionless co-ordinate;
μ, dynamic viscosity;
ν, kinematic viscosity;
ρ, density.

Subscripts
w, wall;
∞, free stream;
r, reference.

INTRODUCTION

FLOW visualization methods in experimental fluid mechanics are old: for them ample heritage was provided by Reynolds' classical experiments in defining the limits of laminar flow using dye in water.

The research described in the following pages is an attempt to make quantitative one such flow visualization technique; the movement of minute particles in an air stream. The method is particularly suited to small velocities and as such can provide another tool for measurement in a range where conventional pitot tubes and manometers are hampered by viscous effects [1] and extremely small pressure differences.

The method to be investigated in detail in the following sections can be described briefly as follows. Small particles ($d < 6{\cdot}6\ \mu$) are introduced upstream of the measuring station and carried along with the flow. The measuring station is illuminated with a high intensity intermittent spot of light and the trajectories of the particles carried through the light spot are photographed on high speed film. On film the trajectories appear as dotted lines whose spacing is proportional to the particle velocity. Determination of the particle velocity is thus reduced to the measurement of a distance.

To test the proposed method and provide useful information about convective flows as well, an experimental setup was constructed to enable the determination of free convection velocity profiles about a vertical flat plate heated to a uniform temperature. For this case the theory is well established but no measurements of free convection velocity profiles have been reported which exhibit agreement with theory to the extent found, for example, in forced convection laminar flow [2]. The difficulty of the small velocities compounded with the interaction of the thermal and velocity fields has made the

* Publication from the Heat Transfer Laboratory, University of Minnesota.
† Associate Professor.

application of standard velocity measurement techniques difficult. Earlier measurements of velocity profiles were made by Griffiths and Davis [3] with a hot wire anemometer. In 1930, the now classical measurements of Schmidt and Beckmann [4] using Schmidt's quartz fiber anemometer were reported. More recently, free convection velocity profiles in water were measured by Schecter and Isbin [5], Ibl and Müller [6] and Sesonske [7] using a technique similar to that to be discussed here.

In the 1930's, Fage and Townsend [8], studied turbulent water flow by observing the motion of fine particles moving with the flow. A microscope with rotating objective was used and the particles were illuminated with a high intensity carbon arc. Maximum and minimum velocities were measured and apparently incidently, the mean velocities as well. A recent report by Yerman *et al.* [9] and a paper by van Meel and Vermij [10] describes almost the same method as that used herein independently. These authors, however, used water in channel flow instead of air in free convection and photographed only flow patterns about objects inserted in the flow.

The following sections outline the apparatus used, the manner of taking the measurements, the results obtained and comparisons with the results of others. In Appendix II of [11] are discussed the various factors which can affect the measurements. It is there shown that the effects of particle settling velocity, particle velocity equilibrium with the flow, Brownian motion, thermal gradient drift, velocity gradient drift and electrostatic fields are negligible under the precautions taken in the measurements reported here. Appendix II of [11] also contains a detailed error analysis of the measurement system.

DESCRIPTION OF APPARATUS

The apparatus used consisted of three major units: (1) a constant temperature vertical plate outfitted with suitable heating and temperature indicating devices and mounted on a stand providing limited spacial adjustment, (2) an enclosure to contain the heated plate assembly and a box external to the enclosure to contain particle laden air used in the velocity measurements, and (3) a light-source/camera assembly which was used for velocity measurements. The salient features of each of these groups of equipment will be discussed in the following paragraphs.

The heated plate assembly

The essential features of the heated plate assembly are shown in Fig. 1. The plate temperature was monitored by sixteen individually calibrated, manganin–constantan thermocouples. Two additional shielded thermocouples were used to monitor the ambient air temperature. The heater assembly was attached via hinges to a vertical steel pipe which was in turn mounted on a floor stand providing a vertical travel of about 14 in and a horizontal travel perpendicular to the plate surface of about 4 in.

The enclosure and dust box

To house the heated plate assembly and to minimize the influence of room air currents and temperature fluctuations, the enclosure shown in Figs. 2 and 3 was built of $\frac{1}{2}$ in thick gypsum wall board and fitted into a corner of the room in which the tests were to be conducted. The enclosure was provided with four access panels secured in place with turnbuckles. A 6 in gap on the two sides adjacent to the room was left open on the top and bottom of the enclosure. The bottom gap was covered with 50 mesh per inch copper screen and the interior of the enclosure on all four sides was lined with aluminum foil (electrically connected to the heater assembly) beginning about 3 ft above the heated plate and ending about 3 ft below. The copper screen was employed to reduce the effect of stray air currents and the aluminum foil prevented the build up of electric fields which might influence the particle movement (see Appendix II of [11]). Electrical and thermocouple leads were brought out between the access panels on the long side of the enclosure. The light source and camera (see next section) were inserted through holes in the access panels.

In order that dust could be introduced into the enclosure with a minimum of disturbance, a separate box of $\frac{3}{16}$ in fiberboard was constructed to stand adjacent to the enclosure. The dust box was provided with four doors, an access port and an observation window. Three

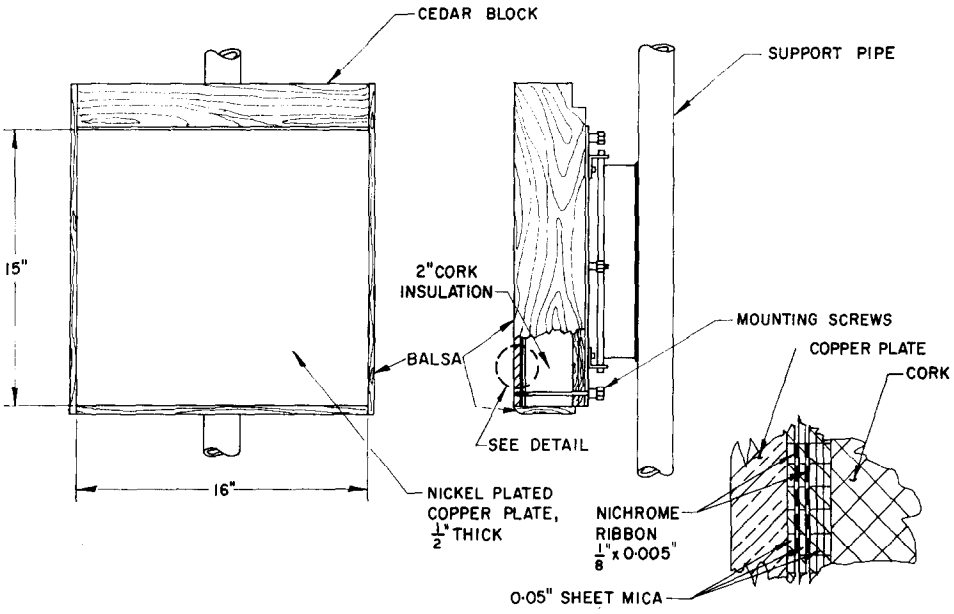

FIG. 1. Heated plate assembly.

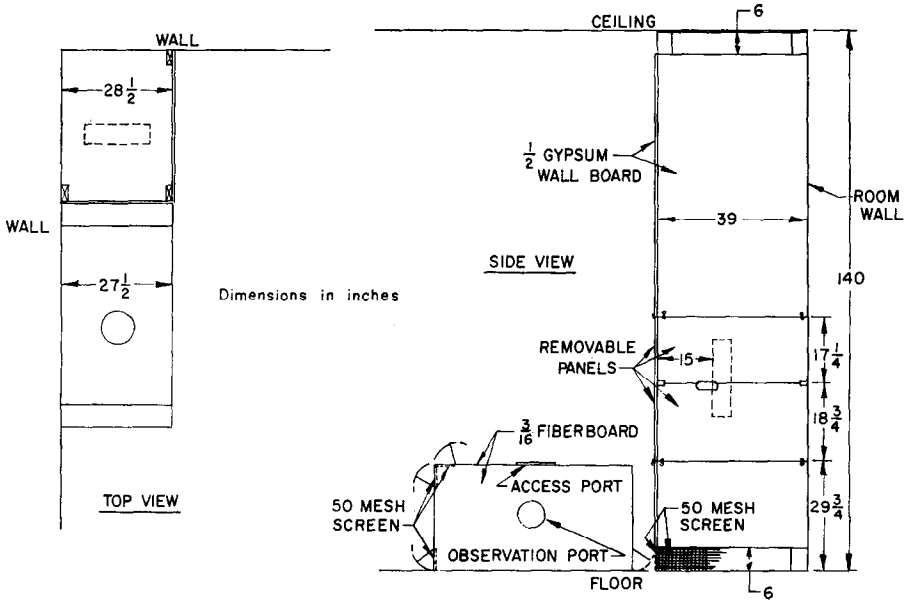

FIG. 2. Heated plate enclosure and dust box.

of the doors opened to the outside room air, the holes thus exposed being covered with 50 mesh per inch copper screen. The fourth door opened in such a way as to connect the dust box directly to the enclosure containing the heated plate.

Light-source/camera assembly

A sketch showing only the principle features of the light-source/camera assembly is shown in Fig. 4. Photographs of the various components are shown in Figs. 3 and 5. The operating principles of this apparatus have already been discussed, here it need only be stated that the dust is carried through the plane of focus of the camera by the action ot the heated air rising about the plate.

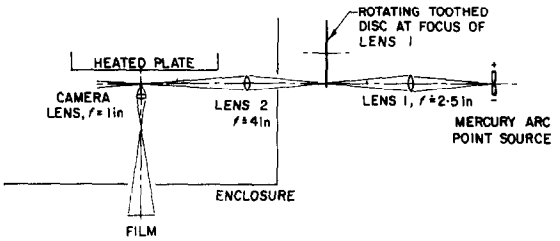

FIG. 4. Principle features of optical system.

Since measurements in a velocity gradient were contemplated, it was necessary to somehow effect pointwise measurements. This may be done by operating the camera lens at apertures and magnifications such that a short depth of field is achieved and/or by illuminating the field of view with a narrow slit of light. The latter method was used by Yerman *et al.* [9] with large particles which could be photographed with relatively slow speed film. With the present apparatus, sufficient light intensity with even a fast film could be obtained only by illuminating the particles ($d < 6{\cdot}6$ μ) with the light beam focused on as small a spot as possible. Since one cannot reduce the size of the light spot at focus with orifices or slits, this method was of no value. The size of the light spot was measured to be about 0·06 to 0·08 in. The limitation to pointwise measurements was, therefore, achieved through the short depth of focus of the camera lens. For the camera setup used, a point source of light (e.g. from a particle) will produce an image of diameter 0·010 in on film if the source is out of the object plane by 0·001 in. Thus if one rejects any images larger than 0·01 in one is assured that the particle is within 0·001 in of the true object plane.

A Prakiflex 35 mm camera with focal plane shutter and ground glass viewing screen was modified for use in this research by substituting for the original lens a movie camera lens (Wollansak CineRaptar, $f/1{\cdot}9$, 1 in focal length) mounted on the end of an 18 in extension tube. The new lens was turned backward to take advantage of the flat field correction of the lens, a technique suggested in [12]. The lens assembly gave a magnification of 17·6 as determined from a Bausch and Lomb micrometer slide and had a field of view of 2·04 by 1·36 mm. The object plane was $\frac{5}{8}$ in from the farthest protruding part of the lens. The camera assembly is shown in Fig. 5.

Light was supplied by a high pressure mercury arc point source lamp* operating at 100 W dissipation and producing a spot 0·3 mm diameter. At the conditions under which this lamp is operated, strong bands of radiation appear in the violet (4358 Å), green (5461 Å and 5780 Å), and infrared (1·015 to 1·7 μ) portions of the spectrum [13]. In photographic processes the violet and green lines are of principal value. The efficiency of the lamp is about 65 lm/W [13] producing a brightness of 73 000 Cd/cm^2 at 100 W dissipation. Power to the light was supplied from the 120 V a.c. mains by a filtered d.c. power supply so the light output was without ripple. The lamp holder provided limited movement in two directions allowing the bright spot to be centered properly with the optical axis of the lens system

The light intercepter was an aluminum disc (mounted outside the enclosure to reduce the effect of stray air currents) 0·02 in thick with sixty radial slots each $\frac{1}{16}$ in wide by $\frac{5}{8}$ in long near the outer edge. The disc was driven at 450 rev/min by a synchronous clock motor. The slot spacing on the disc was uniform to within 0·5 per cent as measured with a Gaertner cathetometer on three sets of six slot spaces at 120° intervals.

* Osram Type, manufactured by Minneapolis Honeywell Regulator Company.

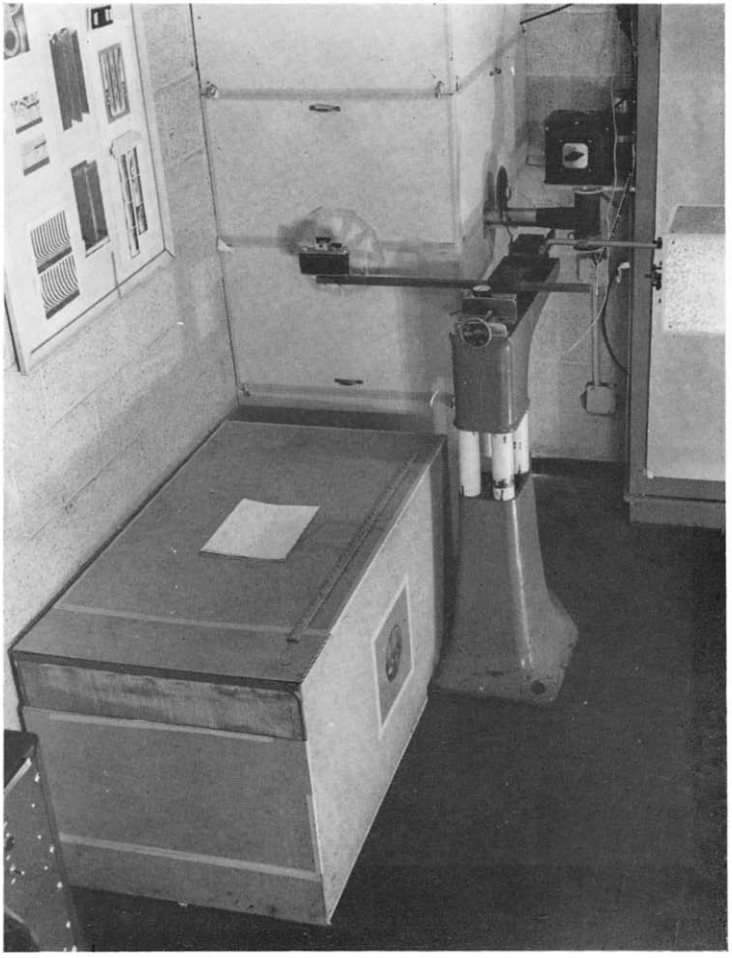

FIG. 3. Photograph of assembled apparatus.

f. p. 918

FIG. 5. Photograph of apparatus (enclosure opened).

With the camera/light-source used, the upper limit on the measurable particle velocity was determined by the possibility of finding two images of the same particle on the film. Since only the brightest portion of the light spot had enough intensity to produce images on the film, and since the projection of the height of the light spot covered only about $\frac{1}{3}$ of the film height or 0·8 cm, the maximum measurable velocity was limited to about $0{\cdot}8(450)/17{\cdot}6 \doteq 20$ cm/s $= 0{\cdot}66$ ft/s for the sixty slot disc.

Two kinds of film were used with the camera, Ansco Super Hypan and Agfa Isopan Record. Both films are high speed (about 500 A.S.A. daylight) with quite fine grain. To obtain as high a speed as possible, the films were developed with Ethol Ultra Fine Grain developer using two to three times the recommended developing time. The results with the Ansco film seemed slightly better with darker images and finer grain. The Agfa film is more sensitive toward the red end of the spectrum than toward the blue where most of the energy of the mercury arc is concentrated. This fact might offer an explanation for the slight superiority of the Ansco film. At the time the measurements were made, the Polaroid films with speeds of 3000 and 10 000 A.S.A. were not available. Consideration of these films in any future experiments is clearly advisable.

The light source and camera were mounted on an optical bench which was itself affixed to a lathe bed external to the enclosure as shown in Fig. 3. The camera extension tube and lens were inserted through a hole in the front of the enclosure such that the extension tube was perpendicular to the heated plate. The final lens tube of the light source was inserted through the other side of the enclosure in a direction parallel to the heated plate surface. The lathe bed was provided with a traversing screw to move the optical bench and thus focus the camera and light source on a plane in the flow parallel to the plate surface. A dial indicator (1 in travel) was mounted on the optical bench and adjusted to read zero with the camera focused on the plate surface. The exact location of the plane of focus was thus determined relative to the plate surface which could be located within about 0·001 in. Since the dial indicator could be read to about 0·0001 in, the location of any particular setting is known to about $\pm 0{\cdot}001$ in.

The light source and camera were placed in alignment by focusing the camera on a 0·001 in glass fiber and adjusting the light source for maximum illumination.

EXPERIMENTAL PROCEDURE

Initially, attempts were made to photograph the dust particles already present in the air. This attack proved fruitless for either the particles were too small or too few to be photographed. With the construction of the dust box it was at least possible to generate clouds of dust with a minimum of disturbance to the plate environment. In the initial measurements, it was found that with the dust box connected to the enclosure, the dust would be blown out of the box into the room about as often as it was drawn into the enclosure. This effect was attributed to a general downdraft through the plate enclosure caused by circulation currents in the room. On the occasions in which the dust was drawn into the enclosure and measurements were made, the velocities close to the surface agreed quite well with theory but the measurements in the outer portions of the boundary layer were erratic and indicated the presence of a general updraft in the plate enclosure. Moreover, observation of the particles in the outer portion of the boundary layer through the viewing lens of the camera indicated that the particles rarely proceeded straight up the plate but often moved in an inclined direction and occasionally even reversed their direction of motion and moved downwards.

In order to remove this troublesome and error-fraught condition, the enclosure was completely closed except for the opening adjacent to the dust box. The joints around the access panels were taped and special precautions were taken to seal the ports through which the camera and light tubes were inserted. Although the sealed enclosure, because of its limited size, now only approximated the conditions for which analytical solutions are available, a closer approximation would require considerable redesign of the enclosure providing a large, nearly air tight, isothermal room.

In all the measurements reported herein, the dust used was zinc stearate, a white compound

in the form of small particles. The particle size distribution for this dust indicated that approximately 90 per cent by volume of the particles were below 7·0 μ in size.

Two sets of measurements are reported in the next section. In the first, dust was blown into the dust box through the access port in the top while the dust box and plate enclosure were connected together. The upper door on the left side of the enclosure was then opened and the dust allowed to settle for 45 min. In the second measurement, the dust was introduced into the dust box while the latter was completely closed. After 10 min the box was connected to the dust enclosure and the upper left side door was opened to the room. In the first case, taking the height of the enclosure and in the second case, the height of the dust box, we can calculate from Stoke's drag equation that particles less than about 6·6 μ will have settled out before the photographs were taken. This is a conservative calculation, and it is doubtful if particles this large were actually encountered in the dust photographs.

After the dust was introduced and just before photographs were taken, the thermoelectric e.m.f.'s were recorded and a barometer reading taken. The dust photographs were then made using exposures of from 10 s very near the plate to 30 s far from the plate. The particular exposure time used was decided on the basis of the numbers of particles observed and the nearness to the plate where shorter exposure times were necessary due to spurious light reflected from the plate surface. Times of the order of 40 min were required to make a complete set of measurements.

The dust photographs were analysed with a Gaertner telemicroscope and micrometer slide. Only the sharpest images were selected for analysis, these being usually less than 0·005 in wide and always less than 0·010 in wide (on film). Where possible, several dust particles on each frame were used.

RESULTS

The experimental results will be presented in three forms: (1) the actual dust photographs, (2) the velocities as calculated from the dust photographs, and (3) the velocities in dimensionless form (equations 1 and 2). The results of two test runs are reported, the essential conditions of each run in Table 1 and the complete data in the Appendix.

Table 1

Run no.	T_w (°F)	T_∞ (°F)	x (in)	Gr_x
1	132·0	80·7	7·0	$1{\cdot}55 \times 10^7$
2	131·8	79·9	3·7	$2{\cdot}30 \times 10^6$

The dust photographs for run 2 are shown in Fig. 6. (The photographs for run 1 were too faint to reproduce satisfactorily.) In both sets of photographs, the particles close to the surface indicate that the flow is vertical with little variation in flow direction. In the outer portions of the boundary layer, however, the flow direction is somewhat erratic. In run 1 (not shown) most of the particles which are skewed appear to be skewed in one direction only. Actual observation of the particles through the camera viewing lens, however, showed this impression to be false. Rather, the particles move in all directions from the vertical with changes in flow direction occuring only very slowly. The situation observed in Fig. 6 is, in this regard, closer to the true situation.

The velocity profiles as determined from the dust photographs are shown in Fig. 7. Where it was possible to analyse more than one particle on a single photograph and the range of velocities so obtained was appreciable, this range is shown by a vertical line and the average value as a point. The data given in the Appendix lists the maximum, minimum and average velocities, and the number of particles analysed in each frame. In all cases the vertical component of the velocity is reported.

In Appendix II of [11] the calculated maximum indeterminant error for measurements of the same velocity is shown to be $\Delta u/u = \pm 3{\cdot}16$ per cent. A further error (less than $\pm 1{\cdot}3$ per cent) is contributed by the depth of field range ($\pm 0{\cdot}001$ in) which can be expressed as $(\Delta y/u)(\mathrm{d}u/\mathrm{d}y)$. Only occasionally are these errors exceeded by the actual measurements.

In run no. 1 the measurements near the peak of the velocity curve are less accurate than the rest since these velocities approach in magnitude

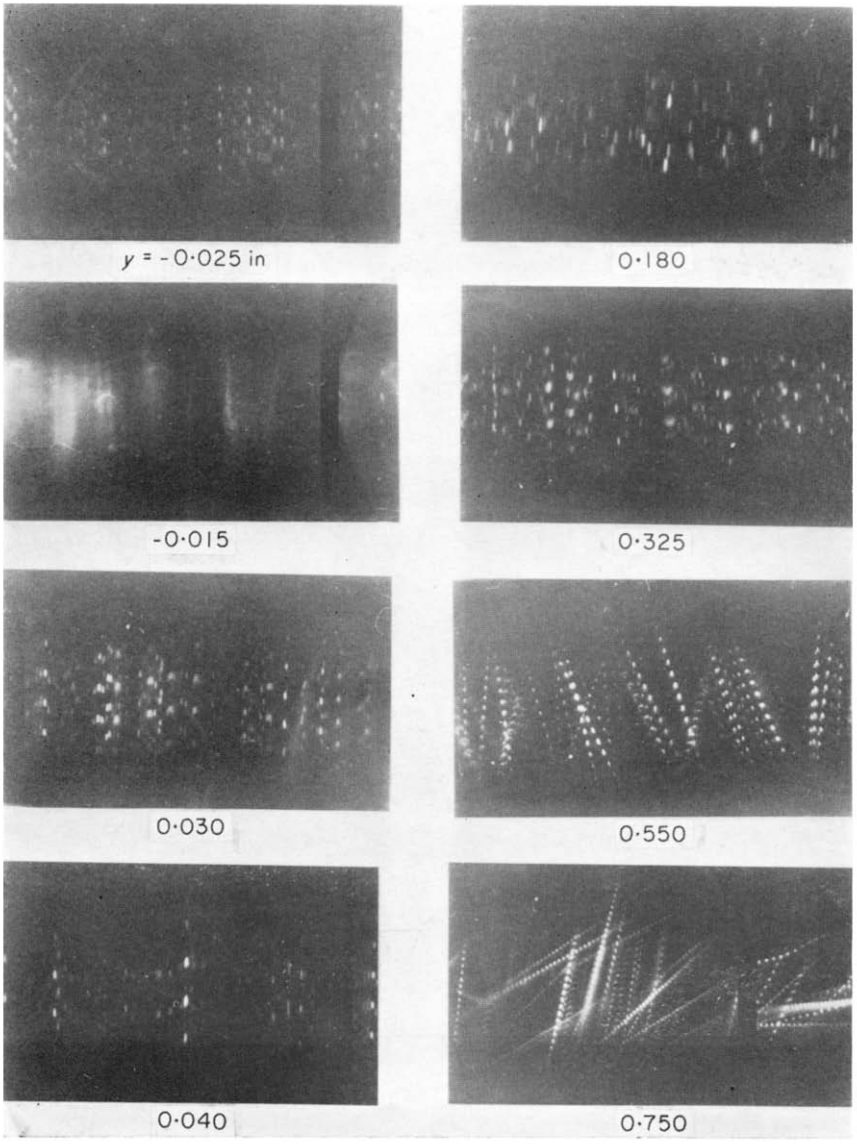

FIG. 6. Sample dust photographs (run 2).

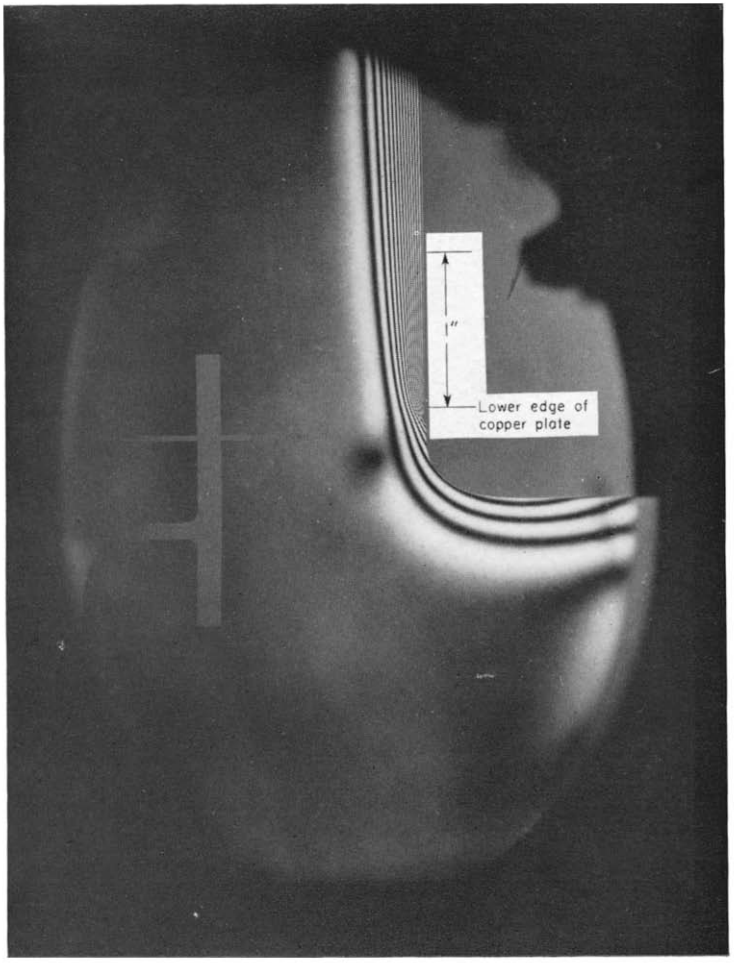

FIG. 9. Interferogram of plate leading edge.

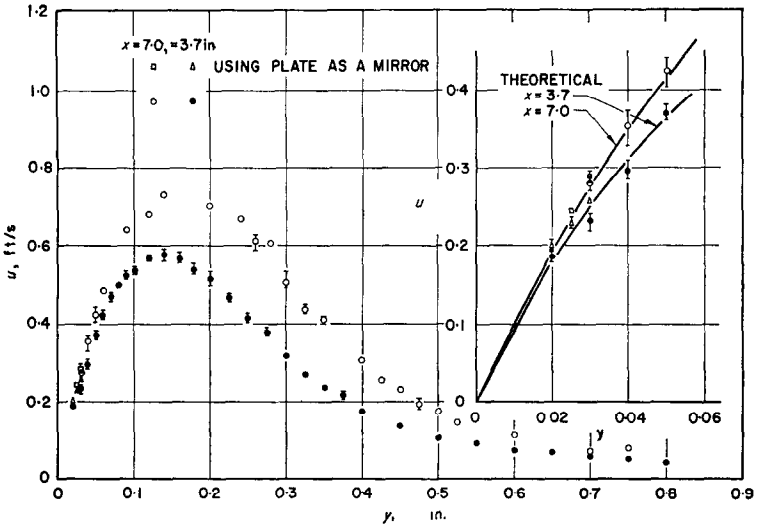

FIG. 7. Velocity profiles.

the upper velocity limit of the apparatus (due to the requirements of photography, see Description of apparatus).

Two points in run no. 1 and three points in run no. 2 were obtained with the camera focused on a point behind the plate surface using the mirrored surface to record data in the flow. The results of these measurements are in quite good agreement with the rest of the data. The insert in Fig. 7 shows this fact more clearly. The theorectical curves shown were taken from [14] with the kinematic viscosity evaluated at a reference temperature as discussed below.

Where possible it is always advantageous to compare experimental data with the corresponding theory. To make this comparison here, the theoretical velocity profiles as obtained from the constant property boundary layer equations will be used. Since the property values are not truly constant, the question arises as to where the property values should be evaluated to effect the best comparison with theory.

The dimensionless velocity profile can be written in the form [14]

$$\zeta'(\eta) = \frac{ux}{4\nu(Gr/4)^{1/2}} = \frac{u}{[4g\beta(T_{\ell} - T_{\infty})x]^{1/2}} \quad (1)$$

where the dimensionless distance from the wall is

$$\eta = \frac{y}{x}\left(\frac{Gr}{4}\right)^{1/4} = \frac{y}{(2)^{1/2}}\left(\frac{g\beta(T_w - T_{\infty})}{\nu^2 x}\right)^{1/4}. \quad (2)$$

Equation 1 contains only the property value β, which for a perfect gas should properly be evaluated as $1/T_{\infty}$. In equation (2) however, the kinematic viscosity ν appears and it is about this quantity that most of the controversy has settled. Schmidt and Beckmann [4] evaluated ν at the wall temperature reasoning that the principal effect of viscosity occurs close to the wall. Ostrach [14] in a re-analysis of Schmidt and Beckmann's data pointed out that the use of ν evaluated at T_w provides good agreement for the temperature profiles but poor agreement for the velocity profiles in comparison with the constant property theory. Accordingly, Ostrach presented plots of the data in [2] using ν_{∞} in equation (2). The velocity profile correlation is somewhat improved but the temperature profiles now disagree quite strongly with theory.

The problem of free convection with variable properties has recently been treated rather completely by Sparrow and Gregg [15] who considered not only gases but liquid mercury as well. For gases over a range of T_w/T_{∞} from 0·25 to 4·0, their results indicated that heat transfer calculated from the constant property solutions using a reference temperature given by

$T_r = T_w - 0{\cdot}38(T_w - T_\infty)$ was within 0·6 per cent of the true value. The skin friction, the location of the maximum velocity, and the approximate thickness of the thermal boundary layer were given by the constant property solutions with reference temperatures computed from the above equation with the coefficient 0·38 replaced by 0·10, 0·24 and 0·67 respectively. From the point of view of the velocity profiles, it appears from these results that the correct reference temperature is not a constant at all but should vary pointwise throughout the boundary layer, the coefficient in the above equation taking on values from about 0·1 to 0·7. The agreement obtained by Ostrach was thus probably fortuitous and at least close to the wall the physical reasoning of Schmidt and Beckmann appears substantially correct.

To get a clearer idea of the effect of variable properties on the velocity correlation, the coefficient of y on the right-hand side of equation (2) has been computed from the data of run no. 1 for several values of the reference temperature as given by the equation $T_r = T_w - a(T_w - T_\infty)$. The several quantities involved are shown in Table 2. The property values were taken from [16].

In view of the results shown in Table 2 and the comments preceding, it was decided to base the kinematic viscosity on a reference temperature which is midway between the recommendation of Sparrow and Gregg for the skin friction and the point of maximum velocity (given by $a = 0{\cdot}17$ in the above equation; see column 3 in Table 2).

The experimentally determined values of ζ' versus η are shown in Fig. 8 and the Appendix. The theoretical curve in Fig. 8 is for $Pr = 0{\cdot}72$ and was taken from [14] whereas the Prandtl No. in this work was nearly 0·705. The theoretical curve for the correct Prandtl No. was not available, but for a change in Pr from 0·70 to 0·72, the height of the maximum velocity point changes by only 0·7 per cent and the change in the η co-ordinate is even less than that [15]. Had the kinematic viscosity been evaluated at the wall temperature, the experimental points would be shifted by 1·12 per cent toward the axis of ordinates. This would not substantially change the appearance of the data. Evaluation of ν at the free stream temperature would shift the data points away from the axis of ordinates by 7·01 per cent and would worsen the correlation.

The agreement between points by the dust method and the theoretical curve is excellent for both velocity profiles in the region close to the wall. For the region approaching and beyond the maximum velocity, the measurements of both runs depart from the theoretical curve in a systematic manner. In addition, run no. 1 exhibits slightly greater random scatter than run no. 2. As mentioned earlier, the higher velocity points in run no. 1 ($\zeta' > 0{\cdot}2$) are not too accurate due to the upper velocity limit of the apparatus.

Although velocity fluctuations and direction changes are present in the outer portions of the boundary layer, these would not be expected to give rise to the systematic deviation from theory evident in Fig. 8. Other possible causes which seem much more plausible are; (1) the extent to which the experiments may disagree with theory (both through the validity of the equations themselves and through the boundary conditions applied in their solution) and (2) the possibility of circulation currents within the enclosure.

It is difficult to say to what extent the theory is applicable to the experimental setup since

Table 2

a	0	0·1	0·17	0·24	0·67	1·0
T_r°F	132·0	127·1	123·3	119·7	97·6	80·7
$\nu_r \times 10^5$ ft²/s	20·28	20·00	19·79	19·55	18·28	17·33
η/y in^{-1}	6·27	6·31	6·34	6·39	6·60	6·78
Change in η/y from $a = 0$, per cent	0	0·64	1·12	1·92	5·26	8·13

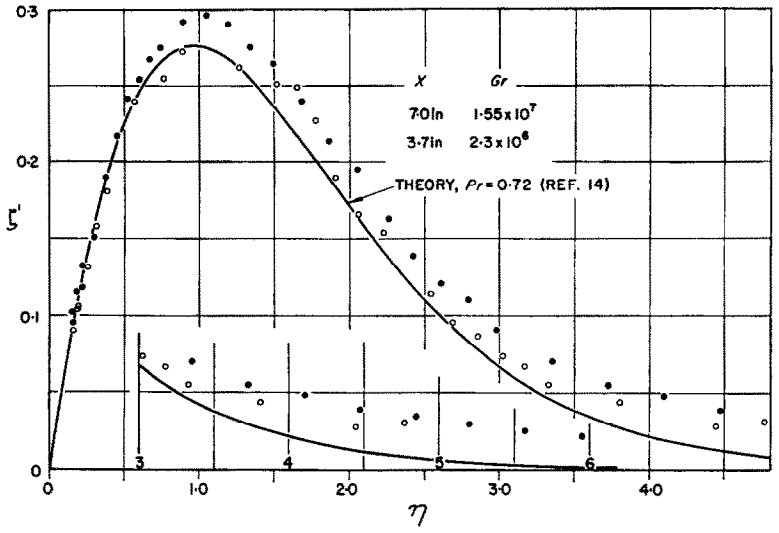

FIG. 8. Dimensionless velocity profiles.

several features of the experiment can readily be seen to disagree with the theory. First, in the derivation of the boundary layer equations themselves, the assumption is made that the boundary layer thickness is smaller by an order of magnitude than the plate length x. For run no. 1, the ratio δ/x was approximately 0·1 and for run no. 2 was about 0·2. In forced flow over flat plates, such ratios of boundary layer thickness to plate length correspond to Reynolds Nos. of 2500 and 625 respectively. In the usual forced flow situations, such Reynolds Nos. are extremely small. The writer is not aware of measurements of velocity profiles in this range. Measurements of temperature profiles, on the other hand, both with thermocouple probes [4] and the Zehnder–Mach interferometer [17] have produced excellent agreement with boundary layer theory at even smaller Grashof Nos. than used here. This fact is not too relevant, however, since the temperature profiles are quite insensitive to small changes in the velocity profiles.

The fact that the theory assumes a plate of infinite width while the experimental plate is only 16 in wide is not believed serious. Considerations by Eckert and Soehngen [17] indicated that at least the thermal field in the center of the plate should be nearly the same as for an infinite plate.

The leading edge boundary condition in the experiment also differs from that in the theory which assumes that heating begins abruptly at $x = 0$. Actually, the balsa slab which attaches to the plate leading edge is slightly heated by conduction from the plate and thus causes the boundary layer to start from a point further upstream. This effect is evident in Fig. 9 which shows an interferogram of the lower portion of the heated plate taken under approximately the same conditions as the velocity runs. The distances which have been listed up to now were measured from the lower edge of the heated plate. Fig. 9 shows quite clearly that the boundary layer extends all around the lower end of the plate assembly. For the conditions of Fig. 9, a shift of one fringe corresponds to a temperature change of approximately 3°F.

It is difficult to estimate the magnitude of the effect of the preheating of the air approaching the boundary layer. At best, perhaps, one can state that the velocities will be higher and that the effect will decrease as x increases.

To check the effect of the preheating on the forms of the velocity profiles, a fictive length was determined for run no. 2 such that the measured maximum velocity was forced to agree with theory. This length, 4·2 in was then used instead of the measured length, 3·7 in in equations 1 and

2 to effect a comparison with theory. Also for run no. 1, the effective starting length thus determined (0·5 in) was assumed to apply and that run recalculated using $x = 7{\cdot}5$ in instead of 7·0 in. The corrected results are shown in Fig. 10.

The agreement with theory is now rather good for both runs up to about $\eta = 3{\cdot}2$ for run no. 1 and $\eta = 2{\cdot}4$ for run no. 2. Beyond these values of η, the data again begin to depart systematically from the theoretical curve indicating the presence of other complicating factors. It seems safe to say that some of the initial disagreement was due to a starting length effect, but whether or not the proper starting length was used in Fig. 10 is open to question. If an updraft in the enclosure is to give rise to some of the effects noted, as will be discussed in the following paragraph, then probably forcing agreement between experiment and theory as was done here for run no. 2 has over-corrected both runs.

The room in which the experiments were conducted was not ideally suited since rarely does the air temperature remain constant even for periods of time as short as 1 h and circulation currents are almost always present caused either by the room temperature changes or the vagaries of the outside weather since the windows seal poorly. Thus one would expect circulation currents within the enclosure caused by temperature fluctuations outside. These facts present a plausible explanation for the behavior of the velocity profiles at large η. For example, if the plate were subject to a steady, uniform, upward flow of air outside the boundary layer, a combined free and forced convective flow would result with velocity profiles similar to those found here.

From Fig. 8, the data of run no. 1 appear to be approaching a value $u \doteq 0{\cdot}07$ ft/s at large y and the data of run no. 2 a value $u \doteq 0{\cdot}04$ ft/s. For run no. 1 the trend is not sufficiently clear and the actual value approached may be nearer 0·04. Using the latter value for both runs, the quantity Re^2/Gr can be calculated as 0·0009 and 0·0017 for runs 1 and 2 respectively. From the results of [18–21], one would not expect the heat transfer or skin friction to be measurably affected. No theory is presently available against which checks of the combined free and forced convection velocity profiles can be made.

CONCLUSIONS

The experimental program dealt with the development of a method to measure small velocities and the application of this method to the measurement of free convection velocity profiles. The following conclusions are presented:

(1) The usefulness of the method of measuring

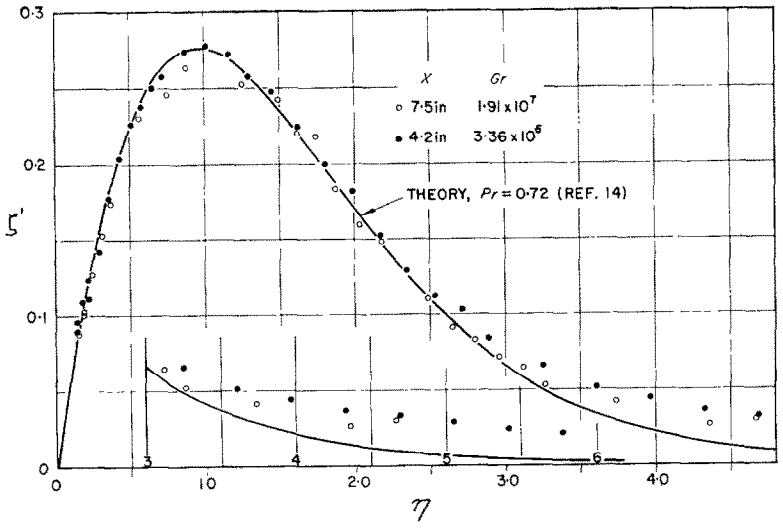

FIG. 10. Dimensionless velocity profiles corrected for starting length.

low fluid velocities by photographing the trajectories of small particles suspended in the flow is demonstrated. An analysis of the various factors which potentially affect the results shows them to be negligible in the cases investigated. The upper velocity limit of the apparatus as constructed is somewhat below the lower limit of conventional velocity measurement techniques but this can be corrected by proper redesign of the apparatus. Within the velocity limits of the apparatus, the accuracy with which a velocity can be measured is not dependent on the velocity itself.

(2) Velocity profiles were measured in the free convection boundary layer and comparison made with theory. At the lower Grashof No. the profiles as measured exhibited a systematic deviation from theory in the region outside the maximum velocity in the boundary layer. At the higher Grashof No. these deviations were less. For the comparison with theory, the kinematic viscosity was based on a reference temperature, $T_r = T_w + 0{\cdot}17(T_w - T_\infty)$ as derived from the analytical work of Sparrow and Gregg [15]. The disagreement between experiment and theory is believed to result from three effects; (a) a starting length effect, (b) disturbing air currents outside the boundary layer, and (c) the failure of the boundary layer equations at small distances from the leading edge. An *ad hoc* starting length correction applied to the data was observed to improve the agreement with theory, but the proper correction and the relative importance of the above three effects is unknown.

ACKNOWLEDGEMENT

Among the several who contributed to the outcome of this research, the writer would like especially to acknowledge the helpful suggestions of Professor E. R. G. Eckert.

REFERENCES

1. R. C. Dean, *Aerodynamic Measurements*. Eagle Enterprises, Boston (1953).
2. J. Nikuradse, *Laminare Reibungeschichten an der langs angestromten Platte*, Monograph. Zentrale für Wissenshaftliches Berichtswesen, Berlin (1942).
3. E. Griffiths and A. H. Davis, *The Transmission of Heat by Radiation and Convection*, Department of Scientific and Industrial Research, Food Investigation Board, Special Rept. No. 9. H.M.S.O., London (1922).
4. E. Schmidt and W. Beckmann, Das Temperatur- und Geschwindigkeitsfeld von einer Warme abgebenden senkrechten Platte bei naturlichen konvektion. *Forsch. Ing. Wes.* **1**, 391 (1930).
5. R. S. Schechter and H. S. Isbin, Natural-convection heat transfer in regions of maximum fluid density. *J. Amer. Inst. Chem. Engrs* **4**, 81 (1958).
6. N. Ibl and R. H. Müller, Studies of natural convection at vertical electrodes. *J. Electrochem. Soc.* **105**, 346 (1958).
7. A. Sesonske, Velocity and temperature distributions about a horizontal cylinder in free convection heat transfer. *J. Amer. Inst. Chem. Engrs* **7**, 352 (1961).
8. A. Fage, Studies of boundary-layer flow with a fluid-motion microscope. *50 Jahre Grenzschicht forschung*. p. 132, Vieweg, Braunschweig, (1955).
9. A. J. Yerman, A. J. Bialous, B. L. Vondra and M. D. Bloomer, A quantitative three-dimensional flow visualization technique, General Electric Co., General Engineering Laboratory, Rept. No. 59GL36 (1959).
10. D. A. van Meel and H. Vermij, A method for flow visualization and measurement of velocity vectors in three-dimensional flow patterns in water models by using colour photography. *Appl. Sci. Res.* **A10**, 109 (1961).
11. R. Eichhorn, An analytical investigation of combined free and forced convections and a new method to measure free convection velocity profiles. Ph.D. Thesis, University of Minnesota (1959).
12. R. D. Cadle and E. J. Wiggins, Direct photomicrography of air-borne particles. American Medical Assoc., *Arch. Industr. Health*, **12**, 584 (1955).
13. J. D. Cobine, *Gaseous Conductors*. Dover, New York (1958).
14. S. Ostrach, An analysis of laminar free-convection flow and heat transfer about a flat plate parallel to the direction of the generating body force. *N.A.C.A.* Report No. 1111 (1953).
15. E. M. Sparrow and J. L. Gregg, The variable fluid problem in free convection. *Trans. Amer. Soc. Mech. Engrs*, **80**, 879 (1958).
16. J. Hilsenrath, *et al.*, *Tables of Thermal Properties of Gases*, NBS Cir. 564 (1955).
17. E. R. G. Eckert and E. Soehngen, Studies on heat transfer in laminar free convection with the Zehnder-Mach Interferometer. Tech. Rept. No. 5747, U.S.A.F. Air Material Command, Dayton, Ohio (1948).
18. E. M. Sparrow and J. L. Gregg, Bouyancy effects in forced convection flow and heat transfer. *Trans. ASME, J. Appl Mech.* **81**, 133 (1959).
19. A. Acrivos, Combined laminar free- and forced-convection heat transfer in external flows. *J. Amer. Inst. Chem. Engrs*, **4**, 285 (1958).
20. J. R. Kliegel, Laminar free and forced convective heat transfer from a vertical flat plate. Ph.D. Thesis, Univ. of California, Berkeley (1959).
21. E. M. Sparrow, R. Eichhorn and J. L. Gregg, Combined forced and free convection in a boundary layer flow. *Phys. of Fluids*, **2**, 319 (1959).

APPENDIX

Results of Dust Photograph Analysis

Run no. 1, $x = 7{\cdot}0$ in, $T_w = 132{\cdot}0°\text{F}$, $T_\infty = 80{\cdot}7°\text{F}$, $Gr = 1{\cdot}55 \times 10^7$

Frame	y in	u_{min} ft/s	u_{avg}	u_{max}	No. of particles used	Avg. no. images per particles	η	ζ'
1*	− 0·030	0·280	0·287	0·295	4	3	0·190	0·107
2	− 0·025		0·244		1	4	0·158	0·091
3	− 0·020				0			
4	− 0·015				0			
5	− 0·010				0			
6	− 0·005				0			
7	0·010				0			
8	0·020				0			
9	0·030	0·271	0·280	0·288	4	3	0·190	0·105
10	0·040	0·329	0·354	0·374	5	2	0·254	0·132
11	0·050	0·404	0·425	0·442	5	2	0·317	0·159
12	0·060	0·479	0·485	0·497	3	2	0·360	0·181
13	0·070				0			
14	0·080				0			
15	0·090	0·639	0·641	0·643	2	2	0·571	0·240
16	0·100				0			
17	0·120		0·681		1	2	0·761	0·255
18	0·140		0·730		1	2	0·888	0·273
19	0·160				0			
20	0·180				0			
21	0·200		0·700		1	2	1·268	0·262
22	0·220				0			
23	0·240		0·670		1	2	1·522	0·251
24	0·260	0·588	0·612	0·626	3	2	1·648	0·229
25	0·280		0·606		1	2	1·775	0·227
26	0·300	0·498	0·509	0·532	5	2	1·902	0·190
27	0·325	0·434	0·444	0·450	5	2	2·060	0·166
28	0·350	0·401	0·412	0·420	2	2	2·219	0·154
29	0·400	0·306	0·308	0·310	4	3	2·540	0·115
30	0·425	0·250	0·256	0·262	5	3	2·694	0·096
31	0·450	0·228	0·233	0·236	4	3	2·853	0·087
32	0·475	0·184	0·198	0·206	3	3	3·012	0·074
33	0·500	0·173	0·180	0·181	4	4	3·170	0·067
34	0·525		0·148		1	5	3·328	0·055
35	0·550				0			
36	0·600	0·114	0·117	0·120	2	6	3·804	0·044
37	0·650				0			
38	0·700	0·071	0·074	0·078	3	9	4·438	0·028
39	0·750		0·082		1	9	4·755	0·031

* Frames 1–6 were taken with camera focused behind plate using plate surface as a mirror.

Run no. 2, $x = 3{\cdot}7$ in, $Gr = 2{\cdot}30 \times 10^6$

Frame	y in	u_{min} ft/s	u_{avg}	u_{max}	No. of particles used	Avg. no. images per particles	η	ζ'
1*	− 0·030	0·258	0·259	0·260	2	4	0·224	0·133
2	− 0·025	0·224	0·229	0·234	2	3	0·186	0·117
3	− 0·020	0·192	0·201	0·208	3	3	0·149	0·103
4	− 0·015				0			
5	− 0·010				0			
6	− 0·005				0			
7	0·010				0			
8	0·020	0·180	0·188	0·196	2	4	0·149	0·096
9	0·030	0·218	0·233	0·242	4	4	0·224	0·119
10	0·040	0·286	0·296	0·310	4	3	0·298	0·152
11	0·050	0·361	0·371	0·382	5	2	0·372	0·190
12	0·060	0·415	0·423	0·435	4	2	0·447	0·217
13	0·070	0·455	0·472	0·475	3	2	0·521	0·242
14	0·080	0·495	0·498	0·502	3	2	0·596	0·255
15	0·090	0·515	0·524	0·536	5	2	0·670	0·268
16	0·100	0·532	0·537	0·543	5	2	0·745	0·275
17	0·120	0·566	0·570	0·577	3	2	0·894	0·292
18	0·140	0·560	0·578	0·592	4	2	1·043	0·296
19	0·160	0·555	0·566	0·581	4	2	1·192	0·290
20	0·180	0·525	0·536	0·553	4	2	1·341	0·275
21	0·200	0·496	0·515	0·532	5	2	1·490	0·264
22	0·225	0·457	0·469	0·479	6	2	1·676	0·240
23	0·250	0·406	0·416	0·427	3	2	1·862	0·213
24	0·275	0·372	0·380	0·393	6	2	2·049	0·195
25	0·300	0·313	0·319	0·322	5	3	2·235	0·163
26	0·325	0·269	0·272	0·274	4	3	2·421	0·139
27	0·350	0·232	0·237	0·242	5	4	2·608	0·121
28	0·375	0·208	0·216	0·226	5	3	2·794	0·111
29	0·400	0·175	0·178	0·179	5	5	2·980	0·091
30	0·450	0·132	0·137	0·141	4	4	3·352	0·070
31	0·500	0·104	0·108	0·110	5	6	3·725	0·055
32	0·550	0·091	0·093	0·096	3	6	4·098	0·048
33	0·600	0·075	0·076	0·076	2	8	4·470	0·039
34	0·650	0·062	0·069	0·077	3	7	4·842	0·035
35	0·700	0·059	0·060	0·061	2	6	5·215	0·031
36	0·750	0·052	0·052	0·052	2	8	5·588	0·027
37	0·800	0·043	0·043	0·043	2	12	5·960	0·022

* See footnote on page 926.

Résumé—L'auteur présente l'étude d'une méthode de mesure des petites vitesses d'écoulement et son application à la mesure des profils de vitesse de convection libre dans l'air. Cette méthode utilise des techniques photographiques pour mesurer les trajectoires de petites particules de poussière ($d < 6{,}6\ \mu$) en suspension dans l'écoulement. Les facteurs intervenant dans cette technique de mesure et les résultats de mesure de deux profils de convection libre sur une plaque verticale sont étudiés.

Zusammenfassung—Die Entwicklung einer Messmethode für kleine Strömungsgeschwindigkeiten und ihre Anwendung auf Geschwindigkeitsprofile der freien Konvektion von Luft sind beschrieben. Dabei lassen sich die Trajektorien kleiner Staubpartikel ($d < 6{,}6\ \mu$), die in der Strömung mitgeführt werden, photographisch festlegen. Faktoren, die dieses Messverfahren beeinflussen können und Messergebnisse für zwei Geschwindigkeitsprofile bei laminarer freier Konvektion an einer ebenen senkrechten Platte sind angegeben.

Аннотация—В статье описывается метод измерения малых скоростей потока и его применение для определения профилей скорости свободной конвекции. Описываемый метод использует фотографию для измерения траекторий мелких пылевидных частиц ($d < 6{,}6\mu$), уносимых потоком. Обсуждаются причины, влияющие на технику измерений, и приводятся результаты измерений двух профилей скорости ламинарной свободной конвекции на вертикальной пластине.